BUDAPEST UNIVERSITY OF TECHNOLOGY AND ECONOMICS
FACULTY OF MECHANICAL ENGINEERING
DEPARTMENT OF ENERGY ENGINEERING

# Modeling the combustion behavior of biomasses and wastes

Thesis booklet

Tibor Szűcs
Energy Engineer

Supervisor:
Dr. Pál Szentannai
Associate Professor

Budapest, 2021

# 1 Introduction

Solid fuels are one of the oldest energy sources and play an essential role in our lives, starting from the first bonfires. Until the end of the 20th century, fossil fuels dominated, but various renewables became significant with the recent environmental concerns. Renewable is a broad category, including all biomass and waste-derived fuels that (unlike fossil fuels) can restock in a foreseeable timescale.

In addition to their environmental benefits, waste-based fuels are cheaper than most fossils, so they could be desirable alternatives for solid-fuel power plants. However, one of the significant obstacles to their wider spread is their unique flow and combustion properties, varying from coals significantly. As a result, their behavior in the boiler can only be assessed by thorough preliminary examinations, and general guidelines can only be formulated in a limited way. However, it is generally true that the larger the particle and the less spherical it is, the more complex model is required for an accurate description.

Research concerning the rate of combustion reactions can be divided into two groups, the intrinsic and the apparent reaction kinetics. Intrinsic kinetics deals purely with the chemical side of combustion, neglecting all other factors influencing it. At the same time, the apparent kinetics describes the combustion of real-sized particles in realistic conditions. Their connection is quite complex, the internal kinetics is the part of the apparent ones, but they can not be directly linked. This grouping is virtually identical to the classical and formal reaction chemistry used in physical chemistry. The former is concerned with describing homogeneous fluid phase reactions, while the latter relates to heterogeneous reactions with solid phases.

Research on these two topics is essentially carried out in separate ways. Intrinsic kinetics is covered by physical chemistry, usually with minimal respect for industrial application. Also, combustion engineers dealing with apparent kinetics tend to utilize the new theoretical results on intrinsic reaction kinetics with a significant delay.

This thesis aims to review solid fuels' whole combustion process, with questions of intrinsic and apparent kinetics and industrial application as well. First, a design method is presented, which can select (and adjust their proportions) the bed materials needed for the binary bed capable of effectively burn solid fuels tend to fragment. To demonstrate this method, the relevant steps are performed for two non-tire rubber samples.

Then, through the example of an SRF (*solid recovered fuel*) sample, the process of building an intrinsic reaction model is presented. During the procedure, the most commonly used evaluation methods are compared. The effect of the parameters in the reaction equations is also tested using sensitivity analysis.

Finally, a modeling process is developed, covering many solid fuels' apparent combustion kinetics, regardless of size, shape, and origin. As a demonstration, the method is performed for a sunflower shell pellet sample.

# 2 Research methods, results, and thesis

## 2.1 Fluidization of fuels tending to primary fragmentation

### 2.1.1 The investigated phenomena

The combustion of big fuel particles (with a diameter of several cm) is realizable in fluidized bed boilers. In such equipment, the fuel burns in a sand bed, which is in a floating state similar to boiling water. This state is called fluidization, and its primary criterion is that the superficial gas velocity is greater than the minimum fluidization velocity defined by the particle and less than the takeover velocity, where the particle is blown out of the bed. These criteria are valid for both fuel and sand particles, although in industrial applications, the latter's share significantly exceeds that of the former. So the criterion for fluidization of a given fuel includes both the correct selection of the bed material and the superficial gas velocity adjustment.

Chirone et al. described first in detail the processes responsible for the comminution of solid particles and the increased takeover rate because of this. Four phenomena have been identified, among which the most significant is the primary fragmentation. This process occurs in parallel with the volatile release. The gases produced in the particle increase the internal pressure so much that it eventually leads to the particle's rupture.

Binary fluidized beds are a special kind of fluidized bed containing two bed materials with similar shares. The related fundamental scientific principles were established in the '70s by Rowe and Nienow. They observed the characteristic arrangement of bed materials; that can be well mixed or vertically segregated, depending on the material properties and the superficial gas velocity. To describe this behavior, the $M$ mixing index was introduced, which is defined as the ratio of the jetsam particles (that tends to sink) in the homogeneous upper part and the whole bed.

Binary fluidized beds have the advantage that their minimum fluidization velocity can be modified by adjusting the components' ratio. In the case of multiple fuel components, it makes it possible to modify the bed to fluidize all components.

### 2.1.2 The proposed design method

The design process's result is a fluidized bed, in which the original sized and the fragmented components of solid fuels can be fluidized together despite the significant differences in size, which is essential for efficient combustion. Its primary condition is to use bed material that can keep the original-sized particles from sinking with a minimum fluidization velocity less than at which the fragmented components are blown out.

If this is not fulfilled, two operational problems are possible. Either the fragmented fine particles fly out of bed, or the original sized ones sink to the bottom. The former results in fine particles leaving the boiler before they burn out, which means energy loss and increased emissions. In the latter case, a significant part of the heat release would be limited to the bottom resulting in a local temperature peak, which would increase the emissions ($NO_x$) and damage the equipment as well.

Thesis 1 includes the steps of the proposed design method:

## Thesis 1

**Fuels that suffer significant size changes during combustion can be fired efficiently in a binary fluidized bed. The two bed materials can be selected, and their ratio can be set using the following four-step design process (criteria system):**

1. The behavior of the fuel components in the selected bed materials shall be investigated. It needs to be possible for all fuel components to be in a fluidized state in at least one of the bed materials.
2. The two bed materials must be fluidized in a segregated way. The binary fluidized bed is considered to be segregated if the mixing index developed by Nienow is $M < 0.5$.
3. The resulting minimum fluidization velocity of the binary bed shall be less than the fragmented fuel's takeover velocity. It can be achieved by adjusting the ratio of the two bed materials.
4. The original sized fuel must not sink to the bottom. This aspect can be verified by performing a cold fluidized bed experiment.

Suppose the selected bed material pair cannot meet any of the above requirements, new bed materials must be selected, and the procedure must be carried out again.

**Related chapter: 4.1.1**
Demonstration: 4.1.2
Results: 5.1

Related publications: $(1) - (6)$

Step 1 is a necessary but insufficient criterion that excludes the clearly wrong bed materials. Also, the necessity of the binary bed can be verified, as this inspection will reveal if one of the bed materials is enough on its own.

Step 2 checks the adequacy of the bed materials for the original sized fuel particles. This criterion forces the bed material with a larger diameter to stay at the bottom and keep the fuel particles in a fluidized state. This compliance can be checked by calculation, requiring the bed materials' basic material properties and minimum fluidization velocities.

Step 3 is about keeping the fragmented fuel particles in the bed. A cold fluidization experiment is recommended to determine the resulting minimum fluidization velocity.

Step 4 sets the minimum share of the bed material with a larger diameter. It is necessary, as the previous steps would allow to reduce it to a level that would no longer keep the original fuel particles moving.

### 2.1.3 Illustration of the method developed

As a demonstration, the design method was performed on non-tire rubber samples prone to primary fragmentation. Two bed materials, sand, and gravel was selected to co-fluidize the original sized and fragmented fuel particles. Based on the preliminary tests, they both meet the requirements of Step 1.

According to step 2, to keep the particles of the original size in a fluidized state, the bed materials must be fluidized in a segregated way, i.e., the mixing index $M$ must be less than 0,5. This aspect

is illustrated in Figure 1, which shows the mixing indices of the binary fluidized beds with different ratios as a function of the superficial gas velocity. The points satisfying step 2 are below the $M = 0{,}5$ red line.

Step 3 further narrows this area since the mixture's minimum fluidization velocity must be less than the takeover velocity of fragmented particles (0,8 m/s), indicated by the black vertical line. Merging this with Step 2 reveals the range (green rectangle) that contains the minimum fluidization velocities that meet both criteria.

The correct ratio can be determined by iteration. The first test mixture ratio was 50-50%; this should be adjusted by reducing the gravel share ($x_H$) until the resulting minimum fluidization velocity is less than 0,8 m/s. For each mixture tested, the mixing index is determined as a function of the superficial gas velocity, as shown in Fig. 1, together with the minimum fluidization velocities. The 1:1 ratio has a minimum fluidization velocity of 1.08 m/s, which is reduced to 0.9 and 0.76 m/s in the cases of ratios 1:3, and 1:6 (25% and 14.3%), respectively. The latter is less than 0.8 m/s, i.e., the star representing it falls into the green rectangle, so this ratio meets Step 2 and 3 both.

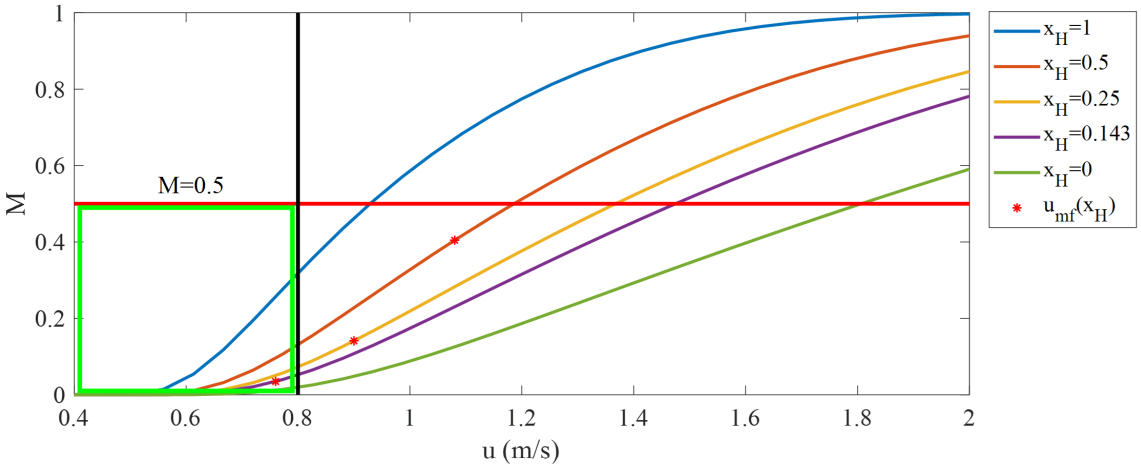


*Figure 1: Mixing index curves for different bed material ratios as a function of the superficial gas velocity with the corresponding minimum fluidization velocities and the aspects of the proposed design method*

The final task is to complete Step 4 since the significantly reduced amount of gravel may no longer keep the rubber particles of the original size fluidized. However, according to the observations, the particles in question are clearly fluidized in the binary fluidized bed.

Based on the above, the design process according to Thesis 1 is suitable for adjusting the binary fluidized bed parameters. In a 1:6 mixture of the bed materials, it is possible to reliably co-fluidize the rubber samples in original and fragmented form.

## 2.2 Intrinsic reaction kinetic model of SRF

The next chapter details different methods capable of building an intrinsic reaction kinetic model for an SRF sample's combustion. The whole modeling process is presented, including the thermogravimetric (TG) measurements, the structure of reaction models based on model-free and model fitting methods with varying complexity, and the optimum seeking algorithm used to determine the reaction kinetic parameters. Furthermore, the precision of the model-fitting methods is compared through the means of sensitivity analysis.

Each method aims to determine the Arrhenius equation's parameters (eq. 1), which represents the progression (conversion, $x$) of a reaction consisting of $N$ sub-reactions as a function of the reaction temperature ($T$). In the equation, $A$ is the preexponential factor, $E$ is the activation energy, $f(x)$ is the reaction function, and $\beta$ is the heating rate.

$$\frac{\mathrm{d}x}{\mathrm{d}T} = \sum_{i=1}^{N} c_i \frac{A_i}{\beta} \, \mathrm{e}^{-\frac{E_i}{\Re T}} f(x_i). \tag{1}$$

### 2.2.1 Model-free methods

The Kissinger-Akahira-Sunose (KAS) and Flynn-Wall-Ozawa (FWO) model-free methods were used with first and second-order reaction functions during the evaluation. Both procedures use the integral form of the Arrhenius equation based on the integral of the reaction function ($g(x)$). Their common feature is that the reaction function is not an output of the methods; it must be determined separately, e.g., with an iterative process.

The KAS method (eq. 2) assumes that if $\ln(\beta/T^2)$ is calculated at specific $x$ values for multiple TG-curves measured with different heating rates, it will result in nearly linear lines, that have the same slope (in the case of single reactions). This slope is $-E/\Re$, where $\Re$ is the universal gas constant, so $E$ can be calculated, and substituting $E$ in eq. 2 gives $A$.

$$\ln\left(\frac{\beta}{T^2}\right) = \ln\left(\frac{A\Re}{Eg(x)}\right) - \frac{E}{\Re T}. \tag{2}$$

Similarly, eq. 3 is used for the FWO method, according to which, $\ln(\beta)$ as a function of $1/T$ for different conversions result in linear lines with a slope of $-1{,}052\ E/\Re$.

$$\ln(\beta) = \ln\left(\frac{AE}{\Re}\right) - \ln\big(g(x)\big) - 5{,}331 - 1{,}052\frac{E}{\Re T}. \tag{3}$$

In the case of complex samples such as SRF, these methods change so that the slope of the lines varies, so different activation energies correspond to different conversion values.

### 2.2.2 Model-fitting methods

In contrast to the model-free methods, model-fitting procedures can determine the reaction function (parallel to the activation energy and the preexponential factor).

Numerical optimum seeking (based on a genetic algorithm) was used to implement the model-fitting methods, in which the goal is to fit a measured conversion graph ($x_\mathrm{m}(t)$) with a calculated one ($x_\mathrm{c}(t)$). The developed genetic algorithm aims to minimize the difference between the two graphs to determine the latter's reaction parameters. The two graphs are compared using a fitness value ($F$) calculated by the fitness function, which is the sum of each measured point's error squares. This fitness function for a series of data measured at $N_\mathrm{f}$ different heating rates and each containing $N_{\mathrm{m,i}}$ measured point is as follows:

$$F = \sum_{i=1}^{N_\mathrm{f}} \frac{\sum_{j=1}^{N_{\mathrm{m,i}}} \left(x_{\mathrm{m},i,j}(t) - x_{\mathrm{c},i,j}(t)\right)^2}{N_{\mathrm{m},i}}. \tag{4}$$

In this case, the model with the lowest $F$ gives the best result.

Four different reaction functions were implemented, a first and an nth order, an extended nth order, and a DAEM (*Distributed Activation Energies Method*) model with Gaussian distribution.

Each reaction model contains three reaction groups (i.e., equivalent sub-reactions), which is typical for SRF samples. The reaction equations describing the models are shown in Table 1.

*11: Reaction models compared*

| Reaction model | Equation | |
|---|---|---|
| **First-order** | $\frac{\mathrm{d}x(t)}{\mathrm{d}t} = \sum_{i=1}^{3} c_i A_i \exp\left(\frac{E_i}{\Re T}\right)(1-x_i)$ | (5) |
| **nth-order** | $\frac{\mathrm{d}x(t)}{\mathrm{d}t} = \sum_{i=1}^{3} c_i A_i \exp\left(\frac{E_i}{\Re T}\right)(1-x_i)^{n_i}$ | (6) |
| **Extended nth-order** | $\frac{\mathrm{d}x(t)}{\mathrm{d}t} = \sum_{i=1}^{3} c_i A_i \exp\left(\frac{E_i}{\Re T}\right)(1-x_i)^{n_i}(x_i+z_i)^{m_i}$ | (7) |
| **DAEM** | $\frac{\mathrm{d}x(t)}{\mathrm{d}t} = \sum_{i=1}^{3} c_i \sum_{j=1}^{l} \int_{E_{j-1}}^{E_j} D_i(E_j)\mathrm{d}E \frac{\mathrm{d}x_j(t,E_j)}{\mathrm{d}t} = = \sum_{i=1}^{3} c_i \sum_{j=1}^{l} \int_{E_{j-1}}^{E_j} D_i(E_j)\mathrm{d}E\, A_i \exp\left(-\frac{E_j}{\Re T(t)}\right)\left(1-x_j(t,E_j)\right).$ | (8) |

Sensitivity analyses have been carried out on the reaction parameters to determine whether the parameters have a significant or marginal effect on the fitness value. Based on this, conclusions can be drawn about which parameters might be fixed and treated as constant to speed up future evaluations. Thesis 2 contains all results of this chapter:

## Thesis 2

To describe the intrinsic reaction kinetics of SRF samples, modelfitting methods based on numerical optimum seeking is recommended. This procedure's error is about one-third of that of model-free methods, even with the simplest first-order reaction functions. The more complex nth-order, extended nth-order, and DAEM functions provide more accuracy, but at the cost of a more complicated structure and higher numerical cost. **For general engineering purposes, the first-order reaction function is recommended** because its accuracy is adequate and its structure is simple.

In such evaluation, **determining the activation energies should be carried out with the utmost precision** because the fitness value's sensitivity to the other parameters is almost negligible. This means that the increased accuracy of more complex models does not require the precise determination of newly introduced parameters; it instead results from the enhanced model structure.

**Related chapters: 5.2.2 and 5.2.3**
Method: 4.2.4

Related publications: (7), (9), (10)

## 2.3 Developing an apparent reaction kinetics model

### 2.3.1 Fundamentals of apparent reaction kinetics

Intrinsic reaction kinetics cannot directly describe real fuel particles' combustion since TG measurements are designed so that no limiting effect is present. Accordingly, intrinsic reaction models do not consider several processes that modify the reaction rate; they are only a theoretical maximum for solid particles' combustion under industrial conditions. An apparent reaction model is needed to describe the real reactions, which expands the intrinsic one with the relevant limiting effects. The most important of these limitations are the particle's size and geometry, the internal temperature distribution, and the oxygen transport that affects the char combustion. Through the example of TG measurements and industrial boilers, the main differences between the two conditions are summarised in Table 2.

*2 2: Main differences between TG measurements and combustion in industrial boilers*

| | **TG measurement** | **Industrial boilers** |
|---|---|---|
| **Particle size** | ground and homogenized | original size and shape |
| **The temperature profile of the particle** | homogeneous due to small particle size and slow heating | heterogeneous because the thermal conduction of the particle slows the heat transfer |
| **internal reaction rate** | identical in the whole particle | it depends on the local temperature |
| **oxygen availability** | the ideal quantity is artificially maintained; due to the small particle size, it is available in the whole sample | often smaller than optimal quantity; available only on the particle's surface |
| **process controlling the devolatilization** | only the reaction kinetics | slow and heterogeneous heat-up, which limits the reaction rate |
| **process controlling the char combustion** | only the reaction kinetics | oxygen transport, which is significantly slower than the reaction |

Based on this, the final part presents a method that can establish a link between intrinsic and apparent reactions. It can be used to model the combustion of most large, non-spherical fuels in industrial boilers.

### 2.3.2 Definition of $\eta_{\mathrm{m}}(x_{\mathrm{app}})$

The apparent conversion of a solid fuel particle, considering the limiting effects, is described by eq. 9, where the $k_{\mathrm{r}}$ reaction rate already includes the conversion-dependent part.

$$\frac{\mathrm{d}x_{\mathrm{app}}(t)}{\mathrm{d}t} = \sum_{i=1}^{N_1} c_i \eta_{\mathrm{m}}\left(x_{\mathrm{app}}\right) k_{\mathrm{r},i}(T, x_i) + \sum_{j=1}^{N_2} \frac{c_j c_{Ox}}{\frac{1}{\eta_{\mathrm{m}}\left(x_{\mathrm{app}}\right) k_{\mathrm{r},j}\left(T, x_j\right)} + \frac{1}{k_{\mathrm{d}}(x_j)}} \tag{9}$$

This means that the apparent conversion is issued as the sum of different reaction groups, which either belong to the volatile release or char combustion. The first includes $N_1$ and the later $N_2$ reaction groups, with mass shares of $c_i$ and $c_j$, respectively.

Char combustion depends on the oxygen transfer, which can be treated similar to parallel resistances. The $k_{\mathrm{d}}$ mass transport coefficient represents this, which is the same unit as the intrinsic reaction rate and has the same role in the equation, but its determination method is different.

The $c_{Ox}$ constant describes the oxygen concentration around the particle, which assumes a linear relationship with the reaction rate. In this case $c_{Ox} = p_{Ox,\mathrm{actual}}/p_{Ox,\mathrm{reference}}$, i.e., the ratio of the oxygen partial pressure in the reference and the actual conditions.

The $\eta_{\mathrm{m}}(\mathrm{x}_{\mathrm{app}})$ is the newly introduced mass-related reaction effectiveness factor; its definition is in Thesis 3:

## Thesis 3

**A clear connection between intrinsic and apparent reaction kinetics can be established using the newly introduced fuel-specific function of apparent conversion, the mass-related reaction effectiveness factor ($\eta_{\mathrm{m}}$).** Its maximum value is 1, which is related to the conditions of the ideal TG-measurements, during which the reactions occur in the whole sample. In most cases, however, $\eta_{\mathrm{m}}$ is much, even several orders of magnitude smaller. Due to the structural changes during particle combustion, its value is monotonously increasing, and at the end of the conversion, it is close to or reaches 1.

It can be interpreted as the ratio of the total and the active weight. This depends primarily on particle fragmentation and pores' formation, which significantly increases the active mass ratio as the conversion progresses.

**Related chapter**: **4.3.1**

Related publications: (8) − (9)

Unlike other conversion functions, $\eta_{\mathrm{m}}$, instead of each reaction group's local conversion, applies to the whole sample's apparent conversion. This is because processes that influence the apparent reaction rate (e.g., changes in the particle size or the pore structure) also occur by the entire particle combustion process.

### 2.3.3 Steps of the modeling process

The process developed combines the results of several measurements and modeling procedures, which are initially relatively lengthy. However, the resulting model is fast and straightforward enough to be used in more complex models, e.g., CFD models.

The purpose of the process is, therefore, to derive $\eta_{\mathrm{m}}(x_{\mathrm{app}})$, which requires every other parameter in eq 9. The steps of this are in Thesis 4:

## Thesis 4

**The following steps can be used to determine the mass-related reaction effectiveness factor for a solid fuel sample:**

1. The intrinsic reaction model ($k_{\mathrm{r}}(T,x)$) of the sample should be developed based on TG-measurements.
2. The apparent conversion ($x_{\mathrm{app}}(t)$) of the sample (i.e., its weight loss during combustion) shall be measured during a macroscopic particle combustion experiment under well-defined conditions.
3. The temperature profile of the sample ($T(t)$) and the oxygen transport around it $k_{\mathrm{d}}(x_{\mathrm{app}})$ should be determined, a reliable method for this is a CFD model.
4. Using all previous data, the following general combustion model (in which $N_1$ and $N_2$ are number of volatile and char components, respectively) can be solved for $\eta_{\mathrm{m}}(x_{\mathrm{app}})$:

$$\frac{\mathrm{d}x_{\mathrm{app}}(t)}{\mathrm{d}t} = \sum_{i=1}^{N_1} c_i \eta_{\mathrm{m}}\left(x_{\mathrm{app}}\right) k_{\mathrm{r},i}(T,x_i) + \sum_{j=1}^{N_2} \frac{c_j c_{Ox}}{\frac{1}{\eta_{\mathrm{m}}\left(x_{\mathrm{app}}\right) k_{\mathrm{r},j}\left(T,x_j\right)} + \frac{1}{k_{\mathrm{d}}(x_j)}}$$

After this, using $\eta_{\mathrm{m}}$ it is possible to model the combustion of the same fuel in any other environment defined by new $k_{\mathrm{d}}(x_{\mathrm{app}})$ and $T(t)$ data.

**Related chapter: 4.3.2**
Demonstration: 4.3.3
Results: 5.3 (Thesis 5)

Related publications: $(8)-(9)$

### 2.3.4 Demonstration of the method

The proposed method's steps have been carried out on sunflower shell pellets originated from a domestic processing plant. The cylindrical samples have a length of $20\pm5$ mm, a diameter of 6 mm, and a weight of about 1 g, so it is clear that significant limitations affect their combustion due to their size.

The intrinsic reaction kinetics in step 1 was developed based on the numerical optimum seeking procedure described in the previous chapter by assuming an extended nth-order reaction model

and considering three reaction groups. These reaction groups refer to drying, volatile release, and char combustion.

According to step 2, the apparent conversion ($x_{\mathrm{app}}(t)$) was measured using a simple macroscopic particle heater equipment.

Following step 3, two CFD models were developed to cover the particle's heat-up and the oxygen transfer around it. The models were built using Comsol 5.3 software, one for the volatile release and one for the char combustion. To define proper boundary conditions and to validate the results, temperature and oxygen measurements were performed.

Step 4 includes substituting the previous results in Eq. 9 and determining $\eta_{\mathrm{m}}(x_{\mathrm{app}})$. A genetic algorithm similar to the one used in the intrinsic evaluation was developed, as a modified version of the Arrhenius equation had to be solved.

To determine $\eta_{\mathrm{m}}(x_{\mathrm{app}})$, it is essential to know its general function form, which requires prior knowledge about the sample. If it is available, it is recommended to look directly for the function's parameters since the optimum seeking algorithm is more efficient with fewer parameters to fit. However, in the case of an unknown sample (as in this demonstration), this function form is unknown. There are several methods for determining it; here, a preliminary run was performed, in which $\eta_{\mathrm{m}}(x_{\mathrm{app}})$ was defined as a series of discrete points. Using these intermediate results, the function form can be concluded, and the fitting procedure for its parameters can be performed.

The function form for the given sample and the values of its parameters are included in Thesis 5:

## Thesis 5

**In the case of sunflower shell pellets, $\boldsymbol{\eta_{\mathrm{m}}(x_{\mathrm{app}})}$ can be described by the following differential function:**

$$\frac{\mathrm{d}\eta_{\mathrm{m}}(x_{\mathrm{app}})}{\mathrm{d}x_{\mathrm{app}}} = A_{\eta} e^{-\frac{E_{\eta}}{x_{\mathrm{app}}}} (1-\eta_{\mathrm{m}})^{n_{\eta}} \left(\eta_{\mathrm{m}} + z_{\eta}\right)^{m_{\eta}}, \text{where}$$

| $A_{\eta}$ | $E_{\eta}$ | $n_{\eta}$ | $m_{\eta}$ | $z_{\eta}$ | $\eta_{\mathrm{m,0}}$ |
|---|---|---|---|---|---|
| $1{,}95 \cdot 10^{5}$ | 7,95 | 1 | $2{,}1 \cdot 10^{-2}$ | $1 \cdot 10^{-4}$ | $2{,}5 \cdot 10^{-3}$ |

**Related chapter: 5.3**

Related publications: (8) − (9)

Among the parameters of the function, $E_{\eta}$ can be interpreted as a threshold conversion similar to the activation energy. Before reaching it, the combustion takes place almost only on the particle's surface ($\eta_{\mathrm{m}} \approx 0$) and after it homogeneously throughout the whole particle ($\eta_{\mathrm{m}} \approx 1$). The former is typical for macroscopic particles, and the latter is the behaviour of finely ground particles.

Note that this is not the simplest function form imaginable; with additional considerations, e.g., sensitivity analysis, several parameters may be omitted. However, this is general enough to be a reasonable initial guess for other samples, thereby greatly simplifying the modeling process.

The function defined in this example is resolved and plotted as a function of the apparent conversion (Fig. 2). It can be concluded that the threshold conversion represented by $E_\eta$ is located at the end of the volatile release. It means that the char combustion's apparent reaction rate is close to the intrinsic kinetics, which is limited by oxygen availability.

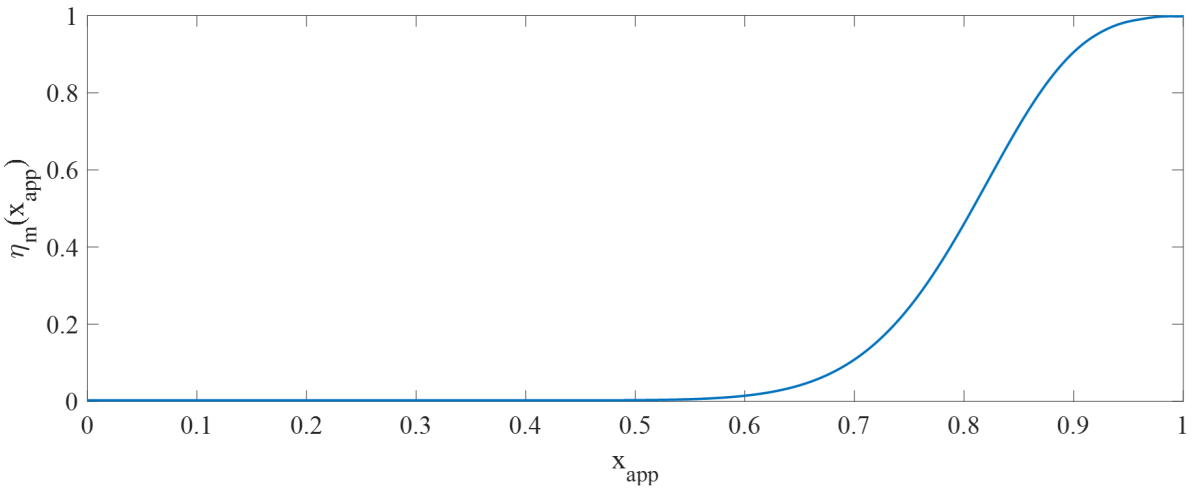


*Fig. 2: The $\eta_m(x_{app})$ function determined for the sunflower shell pellet*

Figure 3 shows the conversion graph calculated with the $\eta_m(x_{app})$ function, compared to the measured data used as the reference of the genetic algorithm. The two curves fit nearly perfectly, so the specified parameters accurately model the behavior of the sample.

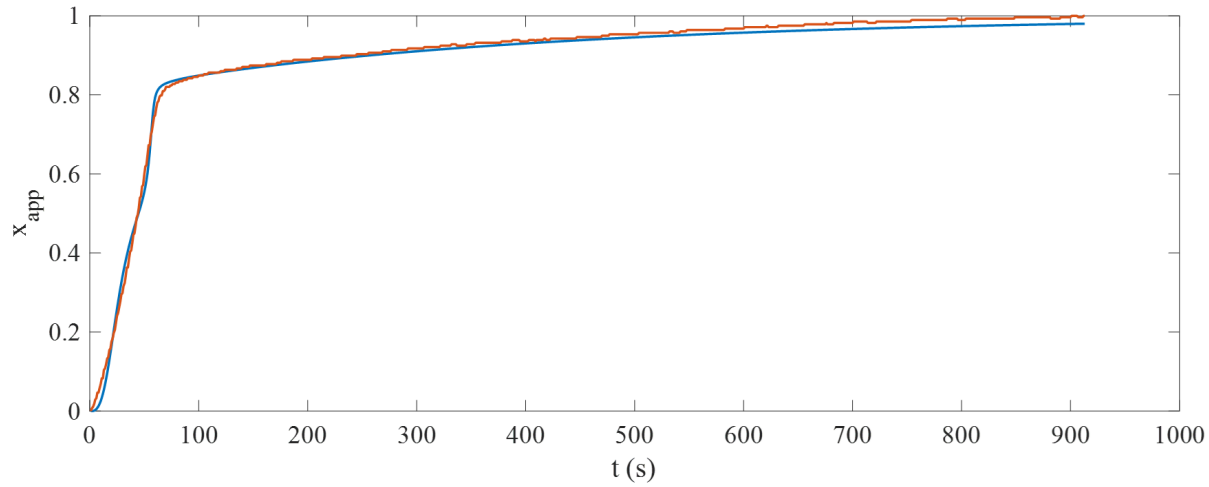


*Fig 3: Apparent conversion curve calculated using the $\eta_m(x_{app})$ (blue) and the measured data (red)*

# 3 Own publications related to the theses

(1) Szentannai, P.; Bozi, J.; Jakab, E.; Ősz, J. and Szűcs, T.: Towards the thermal utilisation of non-tyre rubbers – Macroscopic and chemical changes while approaching the process temperature, Fuel, **156** (2015), pp. 148–157.
*WoS és Scopus adatbázisban; IF: 3,52, Q1*

(2) Szűcs, T.; Jakab, E; and Szentannai, P: Macroscopic and microscopic changes during the combustion process of non-tyre rubber waste particles, 13th International Conference on Heat Engines and Environmental Protection, pp. 177–186, 2017.

(3) Szűcs, T; Szentannai, P: Challenging solid fuels for FBCs, Proceedings of Energy and Environment 2015 19th Annual International Conference, Roznow pod Radhostem, Csehország, pp. 144-148, 2015

(4) Szűcs, T; Szentannai, P: Operational challenges of special solid fuels in fluidized bed boilers, Proceedings on Heat Engines and Environmental Protection Conference (Gyula Gróf), Pécs, ISBN 978-963-313-217-3, 81-88 (2015)

(5) Szűcs, T; Szabó, Z: Egy finn fluidágyas elgázosító üzemeltetési tapasztalatai, Energiagazdálkodás, vol. 55, no. 5–6, pp. 8-11., 2014.

(6) Szentannai, P.; Pláveczky, G.; Sándor, C.; Szűcs, T.; Ősz, J. and Renner, K.: A new design method for fluidized bed conversion of largely heterogeneous binary fuels, Thermal Science, **21** (2017), no. 2, pp. 1105–1118.
*WoS és Scopus adatbázisban; IF: 1,541, Q3*

(7) Szűcs, T.; Szentannai, P.; Szilágyi, I.M. and Bakos, L.P.: Comparing different reaction models for combustion kinetics of solid recovered fuel, Journal of Thermal Analysis and Calorimetry, 139 (2020), no. 1, pp. 555–565.
*WoS és Scopus adatbázisban; IF: 2,471, Q2*

(8) Szűcs, T. and Szentannai, P.: Determining the mass-related reaction effectiveness factor of large, nonspherical fuel particles for bridging between intrinsic and apparent combustion kinetics, Journal of Thermal Analysis and Calorimetry, **141** (2020), no. 2, pp. 797–806.
*WoS és Scopus adatbázisban; IF: 2,471, Q2*

(9) Szűcs, T; Szentannai, P: Developing an all-around combustion kinetics model for nonspherical waste-derived solid fuels, Chemical Papers, Online First, https://doi.org/10.1007/s11696-020-01352-6
*WoS és Scopus adatbázisban; IF: 1,246, Q2*

(10) Szűcs, T. and Szentannai, P.: Hulladékok égésének reakciókinetikai modellezése, Magyar Energetika, **27** (2020), no. 4, pp. 2–8.